HHS Public Access

Author manuscript

Sci Signal. Author manuscript; available in PMC 2016 October 18.

Published in final edited form as:

Sci Signal. ; 9(445): rs10. doi:10.1126/scisignal.aaf7694.

Chemical proteomic map of dimethyl fumarate–sensitive cysteines in primary human T cells

Megan M. Blewett[1], **Jiji Xie**[2], **Balyn W. Zaro**[1], **Keriann M. Backus**[1], **Amnon Altman**[2], **John R. Teijaro**[1,3,*], and **Benjamin F. Cravatt**[1,*]

[1]The Department of Chemical Physiology and The Skaggs Institute for Chemical Biology, The Scripps Research Institute, 10550 N. Torrey Pines Road, La Jolla, CA 92037, USA

[2]Division of Cell Biology, La Jolla Institute for Allergy and Immunology, 9420 Athena Circle, La Jolla, CA 92037, USA

[3]The Department of Immunology and Microbial Science, The Scripps Research Institute, 10550 N. Torrey Pines Road, La Jolla, CA 92037, USA

Abstract

Dimethyl fumarate (DMF) is an electrophilic drug that is used to treat autoimmune conditions, including multiple sclerosis and psoriasis. The mechanism of action of DMF is unclear, but may involve the covalent modification of proteins or DMF serving as a pro-drug that is converted to monomethyl fumarate (MMF). Here, we found that DMF, but not MMF, blocked the activation of primary human and mouse T cells. Using a quantitative, site-specific chemical proteomic platform, we determined the DMF-sensitivity of > 2400 cysteine residues in human T cells. Cysteines sensitive to DMF, but not MMF, were identified in several proteins with established biochemical or genetic links to T cell function, including protein kinase C θ (PKCθ). Furthermore, DMF blocked the association of PKCθ with the costimulatory receptor CD28 by perturbing a CXXC motif in the C2 domain of this kinase. Mutation of these DMF-sensitive cysteines also impaired PKCθ-CD28 interactions and T cell activation, designating the C2 domain of PKCθ as a key functional, electrophile-sensing module important for T cell biology.

Introduction

Dimethyl fumarate (DMF) was first used in the treatment of autoimmunity over half a century ago. In 1959, a German biochemist suffering from psoriasis self-administered DMF, believing his skin condition to be the result of a fumarate deficiency (1). In the 1990s, a mixture of DMF and other fumarates (together known as Fumaderm) was shown to exhibit positive activity in clinical trials for psoriasis. Two multiple sclerosis (MS) patients who had

*Corresponding author. teijaro@scripps.edu (J.R.T.); cravatt@scripps.edu (B.F.C).

Author contributions: M.M.B., J.R.T., and B.F.C. conceived the project; M.M.B. performed the T cell assays and isoTOP-ABPP experiments; M.M.B. and B.W.Z. performed the subcloning and mutagenesis; J.X. performed the PKCθ transduction assays; A.A., J.R.T., and B.F.C. oversaw the project; M.M.B., J.R.T., and B.F.C. drafted the manuscript; and all authors reviewed the manuscript.

Competing interests: The authors declare that they have no competing interests.

Data and materials availability: There are no material transfer agreements or restrictions. All data and materials are freely available. Proteomics data were deposited in XXX with accession number YYY.

been taking Fumaderm for their psoriasis noted that their MS symptoms also stabilized while on the drug. This motivated the clinical investigation of DMF for MS (2-4), and, in 2013, the compound was approved by the FDA as an oral therapy for MS, which is now sold under the trade name Tecfidera (5).

Despite its success in the clinic, the mechanism of action of DMF remains poorly understood. DMF is an electrophilic drug with the potential to react through its Michael acceptor unit with cysteine residues in proteins. Several groups have therefore posited that the drug stimulates an antioxidant response by modifying cysteine residues in the Nrf2-Keap1 complex, a major electrophile-response pathway in mammalian cells (6, 7). Keap1 is a cysteine-rich protein that promotes the proteasomal degradation of Nrf2. Electrophilic or oxidative modification of one or more cysteines in Keap1 causes its disassociation from Nrf2, enabling this transcription factor to bind to antioxidant response elements in DNA and regulate gene expression (6). Others have suggested that DMF acts through the alteration of cellular glutathione (GSH) concentrations, thereby perturbing redox homeostasis (8-11). Alternative models for DMF action have also been put forth, including its ability to serve as a pro-drug for the hydrolyzed product monomethyl fumarate (MMF), which acts as a ligand for the heterotrimeric guanine nucleotide–binding protein (G protein)–coupled receptor (GPCR) hydroxycarboxylic acid receptor 2 (12).

In addition to displaying neuroprotective activity (7, 9), DMF exhibits immunomodulatory properties, including reducing the production of the cytokines interleukin-2 (IL-2), IL-6, and IL-17 by murine splenocyte cultures (9, 13), as well as the production of IL-12 and IL-23 by both mouse and human dendritic cells (14). Reductions in the numbers of $CD4^+$ T cells that express the inflammatory cytokine interferon-γ (IFN-γ) have also been observed in humans taking DMF (14). At least some of the immunosuppressive effects of DMF occur independently of Nrf2 modulation (15) and are not observed with MMF (13), pointing to different proteins and pathways as sites of action for DMF in immune cells. DMF suppresses nuclear factor κB (NF-κB) signaling in different cell types (13, 16-19), which is one potential pathway for immunoregulation, although the mechanism by which this occurs remains poorly understood. These findings, combined with the efficacy of DMF in treating both MS and psoriasis, as well as the emergence of rare, but life-threatening cases of progressive multifocal leukoencephalopathy (PML) among patients taking DMF (20), underscore the importance of elucidating the molecular basis for its immunosuppressive activity.

Our group introduced a chemical proteomic method for quantitatively profiling the reactivity of cysteine residues directly in native cells and tissues (21, 22). Here, we applied this method, termed isoTOP-ABPP (isotopic Tandem Orthogonal Proteolysis-Activity-Based Protein Profiling), to quantify the reactivity of DMF with > 2400 cysteine residues across ~1500 proteins in primary human and mouse T lymphocytes. We discovered numerous cysteine residues that were sensitive to DMF at concentrations at which this drug, but not unreactive structural analogs, suppresses T cell activation. Several proteins harboring DMF-sensitive cysteine residues have established immune regulatory functions. We performed follow-up studies on protein kinase C θ (PKCθ) and showed that a DMF-sensitive CXXC

motif located within its N-terminal C2 domain is critical for interactions with the costimulatory receptor CD28 and for T cell activation.

Results

DMF, but not MMF, inhibits T cell activation

MS is an autoimmune disease with a prominent T cell component (23). We therefore reasoned that DMF might affect primary T cell activation. Consistent with this hypothesis, previous reports showed that DMF inhibits cytokine release from mouse splenocytes (9) and promotes a T helper 2 (T_H2)-type phenotype by causing a modest increase in IL-10 secretion from human and mouse dendritic cells (DCs) (14). We first tested the effects of DMF and MMF (Fig. 1A) on cytokine release from total primary human T cells activated with anti-CD3 and anti-CD28 (anti-CD3/CD28) antibodies. Secretion of IL-2 was substantially inhibited by DMF, but not MMF or the non-electrophilic analog dimethyl succinate (DMS, Fig. 1B). DMF, but not MMF or DMS, also substantially blocked the cell surface expression of the early activation markers CD25 (Fig. 1, C and D) and CD69 (Fig. 1E) in anti-CD3/CD28–stimulated T cells. The blockade of T cell activation by DMF was concentration-dependent, with the drug producing marginal, partial, and near-complete inhibition at concentrations of 10, 25 and 50 μM, respectively (Fig. 1, B to E). Furthermore, the effects of DMF on cytokine release and activation markers occurred at concentrations of the drug that did not impair T cell viability (fig. S1). Similar results were obtained with primary splenic T cells from C57BL/6 mice, the activation of which was also suppressed by DMF, but not MMF or DMS (fig. S2). DMF caused marked inhibition of human T cell activation even when treatment was limited to the first two hours of activation (Fig. 1F), suggesting that DMF inhibits an early event(s) in the T cell activation pathway.

The effects of DMF on T cell activation are independent of Nrf2 and GSH

DMF is thought to produce neuroprotective effects by activating the Nrf2-Keap1 pathway (6, 7), but whether this pathway contributes to the immunomodulatory effects of DMF is unclear. A study showed that DMF inhibits the release of proinflammatory cytokines from primary mouse splenocytes and that this effect is comparable in wild-type and *Nrf2*$^{-/-}$ splenocytes (13). Consistent with this work, we found that the activation of *Nrf2*$^{+/+}$ and *Nrf2*$^{-/-}$ T cells was similarly sensitive to inhibition by DMF (Fig. 2A). DMF might also impair T cell activation by depleting glutathione (GSH), and, indeed, DMF-treated primary human T cells showed a substantial decrease in cellular GSH content (Fig. 2B). Marked reductions in GSH were, however, also observed with the GSH synthesis inhibitor buthionine sulfoximine (BSO), which had no effect on T cell activation (Fig. 2, C and D). These data suggest that the blockade of T cell activation by DMF involves processes other than Nrf2 activation or GSH depletion.

Chemical proteomics reveals DMF-sensitive cysteine residues in T cells

The inhibition of T cell activation by DMF, but not the non-electrophilic analogs MMF and DMS, pointed to a mechanism involving covalent reactivity with one or more proteins important for T cell function. We therefore next sought to identify the DMF-sensitive cysteine residues in primary human and mouse T cells with the quantitative chemical

proteomic platform isoTOP-ABPP. In this method, DMF was evaluated for its ability to block the reactivity of proteinaceous cysteine residues with the general electrophilic probe iodoacetamide-alkyne (IA-alkyne). Using isotopically differentiated azide-biotin tags [containing a tobacco etch virus (TEV) protease–cleavable linker], cysteine residues were identified and comparatively quantified for their IA-reactivity in cells treated with DMF versus DMSO control. The primary advantages of the isoTOP-ABPP platform include: (i) the competing electrophile does not itself need to be chemically altered for target identification, which is particularly beneficial when studying very small compounds like DMF; and (ii) isotopic labeling occurs late in the sample processing, which facilitates the quantitative analysis of primary cells and tissues that are not readily amenable to metabolic labeling.

We performed isoTOP-ABPP on primary human T cells stimulated with anti-CD3/CD28 antibodies and treated with DMSO or 50 μM DMF for 4 hours. Five independent replicate experiments were performed, and the total aggregate number of unique quantified peptides and proteins began to plateau by the fourth and fifth replicate (fig. S3), indicating that we had approached the maximal proteomic coverage of IA-reactive cysteine residues in human T cells that is achievable with the isoTOP-ABPP method under the conditions used. Of the more than 2400 quantified cysteine residues, a small fraction (~40) showed substantial reductions [> four-fold; isoTOP-ABPP ratio (R value) > 4] in IA-alkyne labeling in DMF-treated T cells (Fig. 3A, table S1, and Data file 1). Similar isoTOP-ABPP analyses revealed that none of the ~40 DMF-sensitive cysteine residues was altered by treatment with 50 μM MMF or 2.5 mM BSO for 4 hours, which, in general, affected the reactivity of very few cysteine residues across the T cell proteome (Fig. 3, A and B and fig. S4).

The cysteine residues targeted by DMF exhibited concentration- (Fig. 3C and Data file 1) and time-dependent (Fig. 3D and Data file 1) increases in DMF sensitivity, as revealed by isoTOP-ABPP experiments performed with human T cells that were treated with lower concentrations of DMF (10 and 25 μM, 4 hours; Fig. 3C) or for shorter periods of time (50 μM DMF, 1 or 2 hours; Fig. 3D). Very few DMF-sensitive cysteine residues were detected in T cells treated with 10 μM DMF (Fig. 3C), a concentration of the drug that also had a limited effect on T cell activation (Fig. 1, B to E). These concentration- and time-dependent studies uncovered another ~10 DMF-sensitive cysteine residues that were not detected in the original isoTOP-ABPP experiments (50 μM DMF for 4 hours), likely reflecting the stochastic nature of peptide discovery in data-dependent MS experiments.

We considered the possibility that some of the alterations in cysteine reactivity after treatment with DMF might reflect changes in protein abundance; however, multiple cysteine residues were quantified by isoTOP-ABPP for most of the proteins harboring DMF-sensitive cysteine residues, and, in most of these cases, the additional quantified cysteine residues were clearly unaffected by DMF (Fig. 3E). We showed the DNA-dependent protein kinase catalytic subunit (PRKDC) as one representative example for which IA-alkyne reactivity was quantified for several cysteine residues, only one of which (Cys^{4045}) was blocked by DMF (Fig. 3F). These results suggest that DMF directly impairs the IA-alkyne reactivity of specific cysteine residues rather than indirectly affecting protein abundance in human T cells.

DMF-sensitive cysteine residues are conserved in mice

Considering that DMF impaired the activation of both human and mouse T cells, we surmised that at least a subset of the cysteine residues potentially important for mediating the action of DMF might be conserved in humans and mice. Consistent with this hypothesis, we found that approximately two-thirds of the DMF-sensitive cysteine residues discovered in human T cells are conserved in mice (Fig. 4A and table S1). We next performed isoTOP-ABPP experiments on mouse T cells stimulated with anti-CD3/CD28 antibodies and treated with 50 μM DMF for 4 hours. We found that most (> 80%) of the conserved, quantified cysteine residues that were sensitive to DMF in activated human T cells were also blocked (R values > 4) by this drug in activated mouse T cells (Fig. 4B and Data file 1). These results suggest that DMF targets a similar array of cysteine residues in human and mouse T cells, pointing to a specific set of proteins as the candidate sites of action for this electrophilic drug.

The proteins containing DMF-sensitive cysteine residues, as a whole, originated from several functional classes, including enzymes, channels, transporters, scaffolding proteins, and transcriptional regulators (Fig. 4C). Among these proteins were several with important immune functions (table S1). DMF-sensitive cysteine residues were found, for example, in multiple proteins that are either components or regulators of the NF-κB signaling pathway, including inhibitor of κB (IκB) kinase β (IKKβ or IKBKB) (24), protein kinase C-θ (PKCθ or PRKCQ) (25, 26), and tumor necrosis factor α–induced protein 3 (TNFAIP3, also known as A20) (27, 28) (table S1). Consistent with these, and potentially other, sites of DMF action being within the NF-κB pathway (19), we found that DMF blocked the nuclear translocation of p65 in anti-CD3/CD28–stimulated human T cells (fig. S5), as has been shown in other cell types (13, 16-19). DMF-sensitive cysteine residues were also found in: (i) the adenosine deaminase enzyme ADA, deleterious mutations in which cause severe combined immunodeficiency in humans (29); (ii) the transcription factors interferon regulatory factor-4 (IRF4) and (IRF8); and (iii) the immunomodulatory cytokine IL-16 (table S1). Given its crucial role in early T cell activation, we focused our attention on PKCθ as a case study to begin to understand how DMF affects the function of immunologically relevant proteins in T cells.

DMF perturbs a functional CXXC motif in the C2 domain of PKCθ

PKCθ is a key kinase involved in T cell signaling at the immunological synapse, where engagement of the T cell receptor (TCR) and the costimulatory receptor CD28 initiates the activation of multiple downstream pathways, including NF-κB (25, 26). T cells from PKCθ$^{-/-}$ mice are defective in early activation (30, 31). The isoTOP-ABPP analysis identified two DMF-sensitive cysteine residues in PKCθ, Cys^{14} and Cys^{17}, in human (Fig. 5A) and mouse (fig. S6A) T cells, and these cysteine residues showed time- and concentration-dependent increases in DMF sensitivity (fig. S6, B and C), but were not affected by MMF (fig. S6D). Because Cys^{14} and Cys^{17} are found on the same tryptic peptide, it was difficult to distinguish whether one or both residues were sensitive to DMF. However, in certain isoTOP-ABPP experiments, this tryptic peptide appeared to migrate as two adjacent peaks, both of which showed DMF sensitivity (Fig. 5A), suggesting that the A-alkyne reactivity of both Cys^{14} and Cys^{17} is blocked by DMF. T he isoTOP-ABPP

experiments also identified a third cysteine in PKCθ (Cys^{322}) that was unaffected by DMF (Fig. 5A), indicating that DMF caused reductions in the reactivity of Cys^{14} and Cys^{17} rather than changes in PKCθ abundance.

Cys^{14} and Cys^{17} form a CXXC motif found in the C2 domain of PKCθ, but not other PKC isoforms (Fig. 5, B and C). The C2 domain of PKCθ binds to phosphotyrosine-containing peptides (32) and is postulated to stabilize the plasma membrane association of PKCθ at the immunological synapse (33). Upon stimulation of TCR and CD28, PKCθ is recruited to the immunological synapse where it interacts with CD28 by associating with its cytoplasmic tail (34, 35). We found that DMF, but not MMF, blocked the interaction between PKCθ and CD28 in mouse T cells (Fig. 5D and fig. S7A). We next used retroviral transduction to reconstitute PKCθ$^{-/-}$ mouse T cells with either wild-type PKCθ or a C14S-C17S double mutant PKCθ and found that the mutant protein failed to associate with CD28 (Fig. 5E and fig. S7B). PKCθ$^{-/-}$ T cells reconstituted with the C14S-C17S mutant PKCθ also showed impaired cell-surface expression of CD25 (Fig. 5F) and IL-2 release (Fig. 5G) in response to anti-CD3/CD28 antibodies compared to similarly stimulated cells reconstituted with wild-type PKCθ. DMF further reduced the already impaired ability of PKCθ$^{-/-}$ T cells reconstituted with the C14S-C17S mutant PKCθ to produce IL-2 (Fig. 5H), indicating that the full inhibitory activity of DMF involves proteins other than PKCθ. Combined with previous findings showing that the induced association between PKCθ and CD28 is critical for localizing PKCθ to the center of the immunological synapse (36), our results designate Cys^{14}/Cys^{17} within the C2 domain of PKCθ as a motif that regulates protein-protein interactions that are important for localizing this kinase to signaling complexes in immune cells. Moreover, disruption of this motif by DMF or genetic mutation impairs T cell activation.

Discussion

Considering that DMF is efficacious in two distinct autoimmune conditions—psoriasis and MS—it is reasonable to speculate that the mechanism of action of the drug has a strong immunomodulatory component. The death of a patient in October 2014 due to PML (20) supports this hypothesis; PML is a rare, but serious, viral infection seen almost exclusively in immunocompromised individuals. Consistent with previous studies (13), we showed here that DMF, but not its main metabolite MMF, inhibited the activation of primary human T cells. The inhibitory activity of DMF was also observed in mouse T cells, including T cells from Nrf2$^{-/-}$ animals, but was not displayed by the unreactive analog DMS or by BSO, a pharmacological agent that reduces the amount of GSH in T cells. These results point to a mechanism of action for DMF that involves covalent reaction with proteinaceous cysteine residues in the T cell proteome.

The chemical proteomic method isoTOP-ABPP, by evaluating electrophilic compounds for blockade of IA-reactivity across thousands of cysteine residues in parallel, provided a global way modification to DMF itself. The aggregate number of DMF-sensitive cysteine residues accounted for ~1% of the total cysteine residues quantified in human T cell proteomes, which is a similar degree of proteomic reactivity to that displayed by endogenous lipid electrophiles, such as 4-hydroxy-2-nonenal, which has been similarly evaluated by isoTOP-

ABPP (21). Almost all of the cysteine residues targeted by DMF in T cells showed sensitivity across a concentration range mirroring the range that suppressed T cell activation, with both parameters increasing between 10 and 50 μM (for example, compare Fig. 1, C to E and Fig. 3C). None of the DMF-sensitive cysteine residues in T cells was affected by MMF, which is consistent with previous work showing that DMF reacts much more rapidly with GSH than does MMF (36). These data provide evidence that the reactivity of DMF with cysteine residues is mechanistically relevant to the immunosuppressive activity of the drug.

A substantial number of the proteins harboring DMF-sensitive cysteine residues have established roles in immunology. In the case of PKCθ, which participates in signal transduction pathways that promote T cell activation, we discovered that the DMF-sensitive cysteine residues are important for the TCR-induced association between PKCθ and CD28, which, in turn, localize this kinase to the immunological synapse (36). That these cysteine residues are found in the C2 domain of PKCθ suggests a potentially druggable, non-active site position on this kinase for generating immunosuppressive therapies. Notably, other PKC isoforms, including the closely related PKCδ and PKCε, do not possess the CXXC motif found in PKCθ (Fig. 5B), indicating that the action of DMF is likely restricted to PKCθ over other PKC family members. Moreover, PKCθ-deficient mice are resistant to experimental autoimmune encephalomyelitis (EAE) (37), which suggests that PKCθ-selective inhibitors could have efficacy in MS. Although our data support the idea that disruption of PKCθ function is an important component of DMF action, the ability of DMF to further reduce IL-2 secretion from PKCθ$^{-/-}$ T cells (Fig. 5H) indicates that DMF acts through multiple targets to produce its full inhibitory effect in T cells. These findings point to the potential for covalent drugs to produce biologically important effects through polypharmacology rather than by acting on single targets in cells.

Whether, and how, DMF affects the function of other immunologically relevant protein targets is not yet clear, but we can offer some speculation. For ADA, the DMF-sensitive cysteine residue Cys^{75} is located between two amino acids, Gly^{74} and Arg^{76}, which, when mutated in humans, contribute to an immunosuppressive phenotype (38). The region of ADA formed by amino acid residues 74 to 76 is more than 25 Å from the active site of the enzyme (fig. S8), suggesting that it performs a noncatalytic function that is possibly perturbed by DMF reactivity. The DMF-sensitive cysteine in IKKβ is located in the leucine-zipper domain and is distinct from another electrophile-sensitive cysteine residue, Cys^{179} (39), which is found in the active site of this kinase. We should note that Cys^{179} was not detected in our isoTOP-ABPP experiments, so we cannot conclude whether this cysteine residue is also sensitive to DMF.

Looking forward, it would be interesting to apply the chemical proteomic approach described herein to other cell types to expand our knowledge of DMF action. Discovery of DMF-sensitive cysteine residues in primary neurons, for example, could help to explain the neuroprotective effects of the drug. The isoTOP-ABPP platform could also be used to investigate other cysteine-targeting drugs of ill-defined mechanism, many of which display immunomodulatory activity, for example, curcumin (40) and bardoxolone (41-43), among others. We should also discuss some of the limitations of the isoTOP-ABPP method. Because isoTOP-ABPP quantifies the reduction in the IA-alkyne reactivity of cysteine

residues in the presence of a competing small-molecule electrophile, the method provides robust estimates of high-stoichiometry electrophile-cysteine interactions. On the other hand, low-stoichiometry electrophile-cysteine interactions (< 50% engagement) are more difficult to measure with accuracy. This shortcoming means that isoTOP-ABPP may be better poised to identify electrophile-cysteine interactions that impair, rather than stimulate, protein function, because activating interactions could occur at low stoichiometry. The isoTOP-ABPP method may fail to detect electrophile-sensitive cysteine residues that are found on non-proteotypic peptides; for example, very small, large, or hydrophobic tryptic peptides, or those peptides that exhibit poor reactivity with the IA-alkyne probe. Finally, even though our data suggest that the effects of DMF on T cell activation occur through covalent reactivity, it is possible, and even likely, that the remarkable efficacy displayed by this drug in vivo reflects a multitude of mechanisms, some of which may involve noncovalent interactions of DMF or MMF with proteins that would not be detected by isoTOP-ABPP.

In conclusion, we believe that the chemical proteomic resource provided herein, by revealing not only the proteins, but also the specific cysteine residues on these proteins that are targeted by DMF in primary T cells, provides a strong foundation for mechanistic understanding of the pharmacological activities of this immunosuppressive drug. Those cysteine residues, like Cys^{14}-Cys^{17} in PKCθ, that are found to affect T cell function upon modification by DMF may serve as focal points for future medicinal chemistry efforts aimed at generating covalent ligands with improved potency and selectivity. In this regard, a substantial fraction (~75%) of the DMF-sensitive cysteine residues discovered herein were also identified as targets of structurally distinct fragment electrophiles in a recent isoTOP-ABPP analysis of more than 5000 cysteine residues in human cancer cell line proteomes (44). These fragment electrophiles may thus offer launching points for the development of next-generation immunosuppressive probes and drugs.

Materials and Methods

Chemical reagents

Assays were performed with the following reagents: dimethyl fumarate (DMF; 242926; Sigma Aldrich), monomethyl fumarate (MMF; 651419; Sigma Aldrich), dimethyl succinate (DMS; W239607; Sigma Aldrich), and buthionine sulfoximine (BSO; 14484; Cayman Chemical).

Isolation of primary human T cells

All studies with samples from human volunteers followed protocols approved by the TSRI institutional review board. Blood from healthy donors (females aged 30 to 49) were obtained after informed consent. Peripheral blood mononuclear cells (PBMCs) were purified over Histopaque-1077 gradients (10771; Sigma) according to the manufacturer's instructions. Briefly, blood (20 × 25 ml aliquots) was layered over Histopaque-1077 (12.5 ml) and the samples were then fractionated by centrifugation at 750*g* for 20 min at 20°C with no brake. PBMCs were harvested from the Histopaque-plasma interface and washed twice with phosphate-buffered saline (PBS). After that time, T cells were isolated with an EasySep

Human T Cell Isolation Kit (17951; STEMCELL) according to the manufacturer's instructions.

Mice

C57BL/6J and Nrf2$^{-/-}$ mice (Stock No:017009; Nfe2l2^{tmlywk}; Jackson Labs) were bred and maintained in a closed breeding facility at The Scripps Research Institute and were 6 to 8 weeks old when used in experiments. All mice were used in accordance with guidelines from the Institutional Animal Care and Use Committee of The Scripps Research Institute. For the PKCθ studies, C57BL/6 mice and *Prkcq*$^{-/-}$ mice (a gift from D. Littman) were housed under specific pathogen–free conditions and used in accordance with a protocol approved by the La Jolla Institute for Allergy and Immunology Animal Care Committee.

Isolation of primary mouse T cells

Spleens were harvested from female mice, perfused with collagenase, and incubated at 37°C with 5% CO_2 for 30 min. After this time, the spleens were homogenized. Cells that passed through a 100-μm cell strainer were collected and washed with RPMI. T cells were isolated from the splenocytes with the EasySep Mouse T cell Isolation Kit (19851; STEMCELL) according to the manufacturer s instructions. For the PKCθ studies, CD4$^+$ T cells were isolated by anti-mouse CD4 magnetic particles (L3T4; BD IMag) and were cultured in RPMI-1640 medium (Gibco) supplemented with 10% (vol/vol) heat-inactivated fetal bovine serum (FBS), 2 mM glutamine, 1 mM sodium pyruvate, 1 mM MEM nonessential amino acids, penicillin G and streptomycin (each at 100 U/ml, Life Technologies), and recombinant IL-2 (100 U/ml, Biolegend).

T cell stimulation

96-well plates were coated with anti-CD3 (1:200; BioXcell) and anti-CD28 (1:500; 302933; BioLegend) antibodies in PBS (100 μl per well) overnight at 4°C. The plates were then washed twice with PBS, and to each well was added 500,000 primary T cells in 100 μl of RPMI supplemented with 10% FBS, glutamine, and penicillin-streptomycin. Cells were then treated with 100 μl of medium containing the appropriate compounds at the concentrations indicated in the figure legends (with a final volume of 200 μl per well). Cells were kept at 37°C in a 5% CO_2 incubator for the times indicated in the figure legends and were harvested by centrifugation at 500*g* for 8 min at 4°C, which was followed by washing with PBS.

Cellular analysis and sorting by flow cytometry

Cells were transferred to a round-bottom, 96-well plate (0720095; Fisher Scientific), harvested by centrifugation at 500*g* for 3 min at 4°C, washed with PBS, and stained with LIVE/DEAD fixable cell stain (L23105; ThermoFisher) according to the manufacturer's instructions. Briefly, one vial of LIVE/DEAD stain was resuspended in 50 μl of DMSO and added to 20 ml of PBS. To each well of the 96-well plate was added 200 μl of the diluted stain, and the cells were incubated on ice for 30 min in the dark. After this time, the cells were pelleted and washed once with PBS, and then were incubated with antibodies specific for the appropriate cell-surface markers. Flow cytometric analysis of cell-surface markers was performed with the following antibodies: Pacific Blue–conjugated anti-CD8 (1:25

dilution; clone RPA-T8; BD Biosciences), allophycocyanin (APC)-conjugated anti-CD4 (1:25 dilution; clone RPA-T4; eBioscience), phycoerythrin (PE)-conjugated anti-CD25 [1:25 dilution; clone BC96; eBioscience or PC61; BioLegend (for PKCθ studies)], and fluorescein isothiocyanate (FITC)-conjugated anti-CD69 (1:25 dilution; clone FN50; eBioscience). All antibodies were diluted in PBS, 1% FBS, and 50 μl were added to each well. Cells were incubated for 15 min on ice in the dark, after which the cells were harvested by centrifugation at 500*g* for 3 min at 4°C, washed with PBS, 1% FBS, and resuspended in 200 μl/well of PBS, 4% paraformaldehyde (PFA). Acquisition of flow cytometry data was performed with a BD FACSDiva-driven BD LSR II flow cytometer (Becton, Dickinson and Company). Data were then analyzed with FlowJo software (Treestar Inc.). Data presented in the figures are means ± SEM of four or five experiments per group.

Quantification of secreted cytokines by enzyme-linked immunosorbent assay (ELISA)

T cells were harvested and stimulated as described earlier. At the times indicated in the figure legends, cell culture medium was collected and IL-2 concentrations were measured in clear microplates (991427; R&D Systems) with a Human IL-2 DuoSet ELISA (DY202; R&D Systems) according to the manufacturer's instructions. Plates were read in a Gemini SpectraMax 250 microplate reader set to 450 nm. Data presented in the figures are means ± SEM of four experiments per group. For the PKCθ studies, aliquots of transduced *Prkcq*$^{-/-}$ CD4^{+} T cells (1×10^6) were stimulated for 48 hours with anti-CD3 antibody alone or together with anti-CD28 antibody, and the concentration of IL-2 in the culture medium was determined by enzyme-linked immunosorbent assay (ELISA) according to the manufacturer's instructions (BioLegend). Briefly, a 96-well plate (Corning Costar) was coated overnight at 4°C with anti–IL-2 monoclonal antibody. Triplicates of IL-2 standards and medium from cultured cells were then added to the plate, which was followed by a 2-hour incubation at room temperature. A biotinylated polyclonal antibody against IL-2 was added to the plate, which was followed by incubation for 1 hour at room temperature, and then horseradish peroxidase (HRP)-conjugated avidin (avidin-HRP) was added, followed by incubation for 30 min at room temperature. The amount of bound avidin was then assessed with 3,3′,5,5′-tetramethylbenzidine (TMB) peroxidase that was acidified by 2 N H_2SO_4. The absorbance of each well at 450 nm was then measured with a spectrophotometric plate reader (BioTek).

Quantification of cellular glutathione (GSH) concentrations

Primary human T cells (2.5×10^6 cells/mL, 20 mL per condition) were treated as indicated in the figure legends, harvested by centrifugation at 500*g* for 8 min at 4°C, and washed twice with PBS. To the cell pellet was added 75 μl of lysis buffer (Sigma-Aldrich, CS1020). After being mixed by vortex, the samples were incubated on ice for 15 min and then harvested by centrifugation at 16,000*g* for 10 min at 4°C. Protein concentrations were adjusted to at least 5 mg/ml and the assay was performed according to manufacturer's instructions (Sigma-Aldrich, CS1020). Data are means ± SEM for three or four technical replicates from each of two biological replicates.

Protein labeling and click chemistry

T cells were stimulated and treated in 96-well plates as described earlier. Cells were harvested, lysed by sonication and diluted to a concentration of 2 mg protein/ml. Protein concentrations were measured with the Bio-Rad DC protein assay reagents A and B (5000113, 5000114; Bio-Rad). Proteome sample (500 μl) was treated with 100 μM IA-alkyne probe by adding 5 μl of a 10 mM probe stock (in DMSO). The labeling reactions were incubated at room temperature for 1 hour after which the samples were conjugated to isotopically labeled, TEV-cleavable tags (TEV tags) by copper-catalyzed azide-alkyne cycloaddition (CuACC or "click chemistry"). Heavy click chemistry reaction mixture (60 μl) was added to the DMSO-treated control sample and 60 μl of the light reaction mixture was added to the compound-treated sample. The click reaction mixture consisted of TEV tags [10 μl of a 5 mM stock, light (compound-treated) or heavy (DMSO treated)], $CuSO_4$ (10 μl of a 50 mM stock in water), and TBTA (30 μl of a 1.7 mM stock in 4:1 tBuOH:DMSO). To this was added TCEP (10 μl of a 50 mM stock). The reaction was performed for 1 hour at room temperature. The light- and heavy-labeled samples were then centrifuged at 16,000*g* for 5 min at 4°C to harvest the precipitated proteins. The resulting pellets were resuspended in 500 μl of cold methanol by sonication, and the heavy and light samples were combined pairwise. Combined pellets were then washed with cold methanol, after which the pellet was solubilized by sonication in PBS, 1.2% SDS. The samples were heated at 90°C for 5 min and subjected to streptavidin enrichment of probe-labeled proteins, sequential on-bead trypsin and TEV digestion, and liquid chromatography-tandem mass spectrometry (LC-MS/MS), according to the published isoTOP-ABPP protocols (21, 22, 45, 46).

Peptide and protein identification

RAW Xtractor (version 1.9.9.2; available at http://fields.scripps.edu/downloads.php) was used to extract the MS2 spectra data from the raw files (MS2 spectra data correspond to fragments analyzed during the second stage of mass spectrometry). MS2 data were searched against a reverse concatenated, nonredundant variant of the Human UniProt database (release-2012_11) with the ProLuCID algorithm (publicly available at http://fields.scripps.edu/downloads.php) (47). Cysteine residues were searched with a static modification for carboxyamidomethylation (+57.02146) and up to one differential modification for either the light or heavy TEV tags (+464.28595 or +470.29976, respectively). Peptides were required to have at least one tryptic terminus and to contain the TEV modification. ProLuCID data were filtered through DTASelect (version 2.0) to achieve a peptide false-positive rate below 1% (48).

R value calculation and processing

The quantification of heavy:light ratios (isoTOP-ABPP ratios, *R* values) was performed by in-house CIMAGE software (22) using default parameters (3 MS1s per peak and a signal-to-noise threshold of 2.5). Site-specific engagement of electrophilic compounds was assessed by blockade of IA-alkyne probe labeling. For peptides that showed a ≥95% reduction in MS1 peak area from the compound-treated proteome (light TEV tag) when compared to the DMSO-treated proteome (heavy TEV tag), a maximal ratio of 20 was assigned. Overlapping peptides with the same labeled cysteine (for example, they had the same local sequence

around the labeled cysteines, but had different charge states, MudPIT segment numbers, or tryptic termini) were grouped together, and the median ratio from each group was recorded as the *R* value of the peptide for that run.

Analysis of cysteine conservation

For each human protein containing a DMF-sensitive cysteine, the mouse homolog was identified and the human and mouse sequences were aligned with the Align tool on UniProt.

Immunofluorescent analysis of NF-κB translocation

Primary human T cells (500,000 cells/well) were harvested and stimulated as described earlier, with concomitant treatment with DMSO or DMF for 60 min. Cells were pelleted at 500*g* for 3 min at 4°C, and then the cells in each well were resuspended in 50 μl of PBS and added to poly-D-lysine–coated coverslips (12-mm; 354087; Corning BioCoat). Cells were allowed to adhere to the coverslips for 30 to 60 min at 4°C. The coverslips were then transferred to a 6-well plate and fixed with 4% PFA (157-4-100; Electron Microscopy Sciences) at room temperature for 10 min. After washing three times with PBS, the cells were permeabilized with 0.1% Triton X-100 in PBS at room temperature for 10 min. Cells were washed three times with PBS, and then the coverslips were placed cell-side-up on Parafilm. To each cover slip was added 150 μl of blocking buffer [2% bovine serum albumin (BSA) in PBS], and the slides were blocked for 30 min at room temperature. The blocking buffer was aspirated, and the coverslips were placed face down in 40 μl of antibody buffer [anti-human p65 antibody (p65Ab); FivePhoton Biochemicals; 1:500 dilution in blocking buffer], and incubated overnight at 4°C in a wet chamber. The coverslips were washed three times with PBS and then incubated with 150 μl of secondary antibody (Alexa Fluor 488–conjugated anti-rabbit antibody; A21441; Life Technologies; 1:200 dilution in PBS) for 2 hours at room temperature. After the cells were washed three times with PBS, 150 μl of Hoechst counter stain (5 μg/ml in PBS) were added, and the coverslips were left at room temperature for 30 to 60 min. The cells were again washed three times with PBS and then stained with Alexa Fluor 555–conjugated phalloidin red (8953S; Cell Signaling; 1:20 dilution in PBS). The coverslips were washed with PBS a final three times and then were transferred to SuperFrost Plus slides (12-550-15, Fisherbrand) that were spotted with 10 μl of Prolong Gold Antifade Mountant (P36934, ThermoFisher). The circumference of each coverslip was sealed with clear nail polish (72180; Electron Microscopy Sciences). Images were acquired with a Zeiss 780 laser scanning confocal microscope with a 63× Objective (0.3 μm image step size) and the automated stitching module to merge (10% overlap) and generate a three-dimensional, multi-paneled mega-image composite. The composite image was gathered as a z-series of at least 9 individual image panels that were auto-merged with ZEN software (Zeiss Inc.). The mega-image composite was projected into a maximum image projection in the ZEN software and then was analyzed with the colocalization module in ZEN and Image Pro Premier (Media Cybernetics) software. The Mander's Correlation Coefficients (MCC), specifically M1 and M2 between the various combination of fluorescent label (Alexa Fluor 555–conjugated phalloidin red vs NF-κB-p65 and Hoechst vs NF-κB-p65) were calculated in ZEN per cell and were displayed as percentages. Each cell was outlined using the region of interest module and the software then calculated the M1 and M2 correlation coefficients between the two fluorophores and tabulated the results. The

fluorescent signal dynamic range and threshold cutoff of real signal was defined by multiple background and secondary controls. Correlation coefficient values were compared with Image Pro Premier (IPP) (Media Cybernetics), where images were imported as raw calibrated czi files and analyzed with a similar module in IPP. Similar results were obtained with both platforms. Data represent means ± SEM of two or three biological replicates.

Subcloning and mutagenesis

QuikChange site-directed mutagenesis was performed on a pEF4 His A plasmid containing the cDNA encoding full-length human PKCθ (encoding amino acid residues 1 to 707, courtesy of Amnon Altman and Jiji Xie). The PKCθ insert was excised by digestion with Bam HI and Xho I, and then ligated into a pMIG vector (courtesy of Amnon Altman and Jiji Xie).

Generation of retrovirus encoding PKCθ and transduction and stimulation of cells

Platinum-E packaging cells were plated in a six-well plate in 2 ml of RPMI-1640 medium containing 10% FBS. After 24 hours, the cells were transfected with empty pMIG vector or the appropriate PKCθ-expressing vector DNA (3 μg) with the TransIT-LT1 transfection reagent (Mirus Bio). After overnight incubation, the medium was replaced and the cultures were maintained for another 24 hours. Retroviral supernatants were then collected and filtered, supplemented with polybrene (8 μg/ml), and used to infect $CD4^+$ T cells that had been pre-activated for 24 hours with plate-bound monoclonal antibody against CD3 (8 μg/ml) and CD28 (8 μg/ml). After centrifuging the plates for 1.5 to 2 hours at 800*g*, the supernatants were replaced by fresh RPMI-1640 supplemented with 10% FBS and recombinant IL-2 (100 U/mL). Cells were incubated for another 24 hours at 37°C. The cells were then washed, moved to new plates, and cultured in RPMI-1640 medium containing 10% FBS and recombinant IL-2 (100 U/ml) without stimulation for an 2 additional days before they were restimulated with anti-CD3 antibody alone or together with anti-CD28 antibody.

PKCθ immunoprecipitation and Western blotting analysis

Cells were lysed in 1% (w/v) digitonin (D141, Sigma) lysis buffer [20 mM Tris-HCl (pH 7.5), 150 mM NaCl, 5 mM EDTA] supplemented with the protease inhibitors aprotinin (10 μg/ml), leupeptin (10 μg/ml), and 1 mM PMSF, and with the phosphatase inhibitors 5 mM sodium pyrophosphate and 1 mM Na_3VO_4. Debris was removed by centrifuging the samples at 15,000*g* for 5 min. Supernatants were then incubated for 2 hours with 1 μg of anti-CD28 monoclonal antibody, and proteins were immunoprecipitated overnight at 4°C with protein G-Sepharose beads (GE Healthcare). The immunoprecipitated proteins were resolved by SDS–PAGE, transferred onto a PVDF membrane, and incubated overnight at 4°C with primary antibodies, followed by incubation for 1 hour at room temperature with HRP-conjugated secondary antibodies. Signals were visualized by enhanced chemiluminescence (ECL; GE Healthcare) and were exposed to x-ray film. Densitometry analysis was performed with ImageJ software. Antibodies specific for CD28 (C-20) and PKCθ (C-19) for Western blotting were obtained from Santa Cruz Biotechnology.

Supplementary Material

Refer to Web version on PubMed Central for supplementary material.

Acknowledgments

We thank W. B. Kiosses of the Scripps Research Institute Microscopy Core for assistance with the fluorescence microscopy experiments. We also thank M. Carrillo and N. Nguyen for technical assistance and B. Correia for assistance with filtering the isoTOP-ABPP data.

Funding: This work was supported by the NIH (CA087660) to B.F.C., GM108208 to K.M.B., the Donald E. and Delia B. Baxter Foundation Faculty Scholar Grant to J.R.T., and LEO Pharma. M.M.B. was supported by the NSF Graduate Research Fellowship Program (DGE-1346837) and the Hertz Foundation. B.W.Z. was supported by a Postdoctoral Fellowship, PF-15-142-01 – CDD from the American Cancer Society.

References and Notes

1. Ropper AH. The “;poison chair”; treatment for multiple sclerosis. The New England journal of medicine. 2012; 367:1149–1150. [PubMed: 22992079]
2. Schimrigk S, Brune N, Hellwig K, Lukas C, Bellenberg B, Rieks M, Hoffmann V, Pohlau D, Przuntek H. Oral fumaric acid esters for the treatment of active multiple sclerosis: an open-label, baseline-controlled pilot study. European journal of neurology. 2006; 13:604–610. [PubMed: 16796584]
3. Gold R, Kappos L, Arnold DL, Bar-Or A, Giovannoni G, Selmaj K, Tornatore C, Sweetser MT, Yang M, Sheikh SI, Dawson KT, Investigators DS. Placebo-controlled phase 3 study of oral BG-12 for relapsing multiple sclerosis. The New England journal of medicine. 2012; 367:1098–1107. [PubMed: 22992073]
4. Fox RJ, Miller DH, Phillips JT, Hutchinson M, Havrdova E, Kita M, Yang M, Raghupathi K, Novas M, Sweetser MT, Viglietta V, Dawson KT, Investigators CS. Placebo-controlled phase 3 study of oral BG-12 or glatiramer in multiple sclerosis. The New England journal of medicine. 2012; 367:1087–1097. [PubMed: 22992072]
5. Linker RA, Gold R. Dimethyl fumarate for treatment of multiple sclerosis: mechanism of action, effectiveness, and side effects. Current neurology and neuroscience reports. 2013; 13:394. [PubMed: 24061646]
6. Taguchi K, Motohashi H, Yamamoto M. Molecular mechanisms of the Keap1-Nrf2 pathway in stress response and cancer evolution. Genes Cells. 2011; 16:123–140. [PubMed: 21251164]
7. Scannevin RH, Chollate S, Jung MY, Shackett M, Patel H, Bista P, Zeng W, Ryan S, Yamamoto M, Lukashev M, Rhodes KJ. Fumarates promote cytoprotection of central nervous system cells against oxidative stress via the nuclear factor (erythroid-derived 2)-like 2 pathway. J Pharmacol Exp Ther. 2012; 341:274–284. [PubMed: 22267202]
8. Lin SX, Lisi L, Dello Russo C, Polak PE, Sharp A, Weinberg G, Kalinin S, Feinstein DL. The anti-inflammatory effects of dimethyl fumarate in astrocytes involve glutathione and haem oxygenase-1. ASN neuro. 2011; 3
9. Albrecht P, Bouchachia I, Goebels N, Henke N, Hofstetter HH, Issberner A, Kovacs Z, Lewerenz J, Lisak D, Maher P, Mausberg AK, Quasthoff K, Zimmermann C, Hartung HP, Methner A. Effects of dimethyl fumarate on neuroprotection and immunomodulation. J Neuroinflammation. 2012; 9:163. [PubMed: 22769044]
10. Lehmann JC, Listopad JJ, Rentzsch CU, Igney FH, von Bonin A, Hennekes HH, Asadullah K, Docke WD. Dimethylfumarate induces immunosuppression via glutathione depletion and subsequent induction of heme oxygenase 1. The Journal of investigative dermatology. 2007; 127:835–845. [PubMed: 17235328]
11. Mrowietz U, Asadullah K. Dimethylfumarate for psoriasis: more than a dietary curiosity. Trends Mol Med. 2005; 11:43–48. [PubMed: 15649822]
12. Chen H, Assmann JC, Krenz A, Rahman M, Grimm M, Karsten CM, Kohl J, Offermanns S, Wettschureck N, Schwaninger M. Hydroxycarboxylic acid receptor 2 mediates dimethyl

fumarate's protective effect in EAE. The Journal of clinical investigation. 2014; 124:2188–2192. [PubMed: 24691444]

13. Gillard GO, Collette B, Anderson J, Chao J, Scannevin RH, Huss DJ, Fontenot JD. DMF, but not other fumarates, inhibits NF-kappaB activity in vitro in an Nrf2-independent manner. J Neuroimmunol. 2015; 283:74–85. [PubMed: 26004161]
14. Ghoreschi K, Bruck J, Kellerer C, Deng C, Peng H, Rothfuss O, Hussain RZ, Gocke AR, Respa A, Glocova I, Valtcheva N, Alexander E, Feil S, Feil R, Schulze-Osthoff K, Rupec RA, Lovett-Racke AE, Dringen R, Racke MK, Rocken M. Fumarates improve psoriasis and multiple sclerosis by inducing type II dendritic cells. The Journal of experimental medicine. 2011; 208:2291–2303. [PubMed: 21987655]
15. Schulze-Topphoff U, Varrin-Doyer M, Pekarek K, Spencer CM, Shetty A, Sagan SA, Cree BA, Sobel RA, Wipke BT, Steinman L, Scannevin RH, Zamvil SS. Dimethyl fumarate treatment induces adaptive and innate immune modulation independent of Nrf2. Proceedings of the National Academy of Sciences of the United States of America. 2016; 113:4777–4782. [PubMed: 27078105]
16. Kastrati I, Siklos MI, Calderon-Gierszal EL, El-Shennawy L, Georgieva G, Thayer EN, Thatcher GR, Frasor J. Dimethyl Fumarate Inhibits the Nuclear Factor kappaB Pathway in Breast Cancer Cells by Covalent Modification of p65 Protein. The Journal of biological chemistry. 2016; 291:3639–3647. [PubMed: 26683377]
17. Loewe R, Holnthoner W, Groger M, Pillinger M, Gruber F, Mechtcheriakova D, Hofer E, Wolff K, Petzelbauer P. Dimethylfumarate inhibits TNF-induced nuclear entry of NF-kappa B/p65 in human endothelial cells. Journal of immunology. 2002; 168:4781–4787.
18. Loewe R, Pillinger M, de Martin R, Mrowietz U, Groger M, Holnthoner W, Wolff K, Wiegrebe W, Jirovsky D, Petzelbauer P. Dimethylfumarate inhibits tumor-necrosis-factor-induced CD62E expression in an NF-kappa B-dependent manner. The Journal of investigative dermatology. 2001; 117:1363–1368. [PubMed: 11886496]
19. Peng H, Guerau-de-Arellano M, Mehta VB, Yang Y, Huss DJ, Papenfuss TL, Lovett-Racke AE, Racke MK. Dimethyl fumarate inhibits dendritic cell maturation via nuclear factor kappaB (NF-kappaB) and extracellular signal-regulated kinase 1 and 2 (ERK1/2) and mitogen stress-activated kinase 1 (MSK1) signaling. The Journal of biological chemistry. 2012; 287:28017–28026. [PubMed: 22733812]
20. Faulkner M. Risk of progressive multifocal leukoencephalopathy in patients with multiple sclerosis. Expert opinion on drug safety. 2015; 14:1737–1748. [PubMed: 26394704]
21. Weerapana E, Wang C, Simon GM, Richter F, Khare S, Dillon MB, Bachovchin DA, Mowen K, Baker D, Cravatt BF. Quantitative reactivity profiling predicts functional cysteines in proteomes. Nature. 2010; 468:790–795. [PubMed: 21085121]
22. Wang C, Weerapana E, Blewett MM, Cravatt BF. A chemoproteomic platform to quantitatively map targets of lipid-derived electrophiles. Nat Methods. 2014; 11:79–85. [PubMed: 24292485]
23. Fletcher JM, Lalor SJ, Sweeney CM, Tubridy N, Mills KH. T cells in multiple sclerosis and experimental autoimmune encephalomyelitis. Clinical and experimental immunology. 2010; 162:1–11. [PubMed: 20682002]
24. Karin M, Delhase M. The I kappa B kinase (IKK) and NF-kappa B: key elements of proinflammatory signalling. Seminars in immunology. 2000; 12:85–98. [PubMed: 10723801]
25. Isakov N, Altman A. Protein kinase C(theta) in T cell activation. Annual review of immunology. 2002; 20:761–794.
26. Zhang EY, Kong KF, Altman A. The yin and yang of protein kinase C-theta (PKCtheta): a novel drug target for selective immunosuppression. Adv Pharmacol. 2013; 66:267–312. [PubMed: 23433459]
27. Song HY, Rothe M, Goeddel DV. The tumor necrosis factor-inducible zinc finger protein A20 interacts with TRAF1/TRAF2 and inhibits NF-kappaB activation. Proceedings of the National Academy of Sciences of the United States of America. 1996; 93:6721–6725. [PubMed: 8692885]
28. Wertz IE, O'Rourke KM, Zhou H, Eby M, Aravind L, Seshagiri S, Wu P, Wiesmann C, Baker R, Boone DL, Ma A, Koonin EV, Dixit VM. De-ubiquitination and ubiquitin ligase domains of A20 downregulate NF-kappaB signalling. Nature. 2004; 430:694–699. [PubMed: 15258597]

29. Hershfield, M. Gene Reviews(R). Pagon, RA.; Adam, MP.; Ardinger, HH.; Wallace, SE.; Amemiya, A.; Bean, LJH.; Bird, TD.; Fong, CT.; Mefford, HC.; Smith, RJH.; Stephens, K., editors. Seattle (WA): 1993.
30. Sun Z, Arendt CW, Ellmeier W, Schaeffer EM, Sunshine MJ, Gandhi L, Annes J, Petrzilka D, Kupfer A, Schwartzberg PL, Littman DR. PKC-theta is required for TCR-induced NF-kappaB activation in mature but not immature T lymphocytes. Nature. 2000; 404:402–407. [PubMed: 10746729]
31. Pfeifhofer C, Kofler K, Gruber T, Tabrizi NG, Lutz C, Maly K, Leitges M, Baier G. Protein kinase C theta affects Ca2+ mobilization and NFAT cell activation in primary mouse T cells. J Exp Med. 2003; 197:1525–1535. [PubMed: 12782715]
32. Stahelin RV, Kong KF, Raha S, Tian W, Melowic HR, Ward KE, Murray D, Altman A, Cho W. Protein kinase Ctheta C2 domain is a phosphotyrosine binding module that plays a key role in its activation. The Journal of biological chemistry. 2012; 287:30518–30528. [PubMed: 22787157]
33. Melowic HR, Stahelin RV, Blatner NR, Tian W, Hayashi K, Altman A, Cho W. Mechanism of diacylglycerol-induced membrane targeting and activation of protein kinase Ctheta. The Journal of biological chemistry. 2007; 282:21467–21476. [PubMed: 17548359]
34. Altman A, Villalba M. Protein kinase C-theta (PKCtheta): it's all about location, location, location. Immunological reviews. 2003; 192:53–63. [PubMed: 12670395]
35. Kong KF, Yokosuka T, Canonigo-Balancio AJ, Isakov N, Saito T, Altman A. A motif in the V3 domain of the kinase PKC-theta determines its localization in the immunological synapse and functions in T cells via association with CD28. Nat Immunol. 2011; 12:1105–1112. [PubMed: 21964608]
36. Schmidt TJ, Ak M, Mrowietz U. Reactivity of dimethyl fumarate and methylhydrogen fumarate towards glutathione and N-acetyl-L-cysteine--preparation of S-substituted thiosuccinic acid esters. Bioorganic & medicinal chemistry. 2007; 15:333–342. [PubMed: 17049250]
37. Tan SL, Zhao J, Bi C, Chen XC, Hepburn DL, Wang J, Sedgwick JD, Chintalacharuvu SR, Na S. Resistance to experimental autoimmune encephalomyelitis and impaired IL-17 production in protein kinase C theta-deficient mice. Journal of immunology. 2006; 176:2872–2879.
38. Arrendondo-Vega FX, Santisteban I, Notarangelo LD, El Dahr J, Buckley R, Roifman C, Conley ME, Hershfield MS. Seven novel mutations in the adenosine deaminase (ADA) gene in patients with severe and delayed onset combined immunodeficiency: G74C, V129M, G140E, R149W, Q199P, 462delG, and E337del. Mutations in brief no. 142 Online. Hum Mutat. 1998; 11:482.
39. Kwok BH, Koh B, Ndubuisi MI, Elofsson M, Crews CM. The anti-inflammatory natural product parthenolide from the medicinal herb Feverfew directly binds to and inhibits IkappaB kinase. Chem Biol. 2001; 8:759–766. [PubMed: 11514225]
40. Srivastava RM, Singh S, Dubey SK, Misra K, Khar A. Immunomodulatory and therapeutic activity of curcumin. Int Immunopharmacol. 2011; 11:331–341. [PubMed: 20828642]
41. Gao X, Deeb D, Danyluk A, Media J, Liu Y, Dulchavsky SA, Gautam SC. Immunomodulatory activity of synthetic triterpenoids: inhibition of lymphocyte proliferation, cell-mediated cytotoxicity, and cytokine gene expression through suppression of NF-kappaB. Immunopharmacol. Immunotoxicol. 2008; 30:581–600.
42. Nagaraj S, Youn JI, Weber H, Iclozan C, Lu L, Cotter MJ, Meyer C, Becerra CR, Fishman M, Antonia S, Sporn MB, Liby KT, Rawal B, Lee JH, Gabrilovich DI. Anti-inflammatory triterpenoid blocks immune suppressive function of MDSCs and improves immune response in cancer. Clin Cancer Res. 2010; 16:1812–1823. [PubMed: 20215551]
43. Kitsukawa M, Tsuchiyama H, Maeda A, Oshida K, Miyamoto Y. Immunosuppressive potential of bardoxolone methyl using a modified murine local lymph node assay (LLNA). J Toxicol Sci. 2014; 39:545–550. [PubMed: 25056779]
44. Backus KM, Correia BE, Lum KM, Forli S, Horning BD, González-Paez GE, Chatterjee S, Lanning BR, Teijaro JR, Olson AJ, Wolan DW, Cravatt BF. Proteome-wide covalent ligand discovery in native biological systems. Nature. In press.
45. Weerapana E, Speers AE, Cravatt BF. Tandem orthogonal proteolysis-activity-based protein profiling (TOP-ABPP)--a general method for mapping sites of probe modification in proteomes. Nat Protoc. 2007; 2:1414–1425. [PubMed: 17545978]

46. Weerapana E, Speers AE, Cravatt BF. Tandem orthogonal proteolysis-activity-based protein profiling (TOP-ABPP)--a general method for mapping sites of probe modification in proteomes. Nature protocols. 2007; 2:1414–1425. [PubMed: 17545978]
47. Xu T, Park SK, Venable JD, Wohlschlegel JA, Diedrich JK, Cociorva D, Lu B, Liao L, Hewel J, Han X, Wong CC, Fonslow B, Delahunty C, Gao Y, Shah H, Yates JR 3rd. ProLuCID: An improved SEQUEST-like algorithm with enhanced sensitivity and specificity. J Proteomics. 2015; 129:16–24. [PubMed: 26171723]
48. Tabb DL, McDonald WH, Yates JR 3rd. DTASelect and Contrast: tools for assembling and comparing protein identifications from shotgun proteomics. J Proteome Res. 2002; 1:21–26. [PubMed: 12643522]
49. Pacheco R, Martinez-Navio JM, Lejeune M, Climent N, Oliva H, Gatell JM, Gallart T, Mallol J, Lluis C, Franco R. CD26, adenosine deaminase, and adenosine receptors mediate costimulatory signals in the immunological synapse. Proceedings of the National Academy of Sciences of the United States of America. 2005; 102:9583–9588. [PubMed: 15983379]
50. Cruikshank WW, Center DM, Nisar N, Wu M, Natke B, Theodore AC, Kornfeld H. Molecular and functional analysis of a lymphocyte chemoattractant factor: association of biologic function with CD4 expression. Proceedings of the National Academy of Sciences of the United States of America. 1994; 91:5109–5113. [PubMed: 7910967]
51. Huber M, Lohoff M. IRF4 at the crossroads of effector T-cell fate decision. European journal of immunology. 2014; 44:1886–1895. [PubMed: 24782159]
52. Suzuki S, Honma K, Matsuyama T, Suzuki K, Toriyama K, Akitoyo I, Yamamoto K, Suematsu T, Nakamura M, Yui K, Kumatori A. Critical roles of interferon regulatory factor 4 in CD11bhighCD8alpha- dendritic cell development. Proceedings of the National Academy of Sciences of the United States of America. 2004; 101:8981–8986. [PubMed: 15184678]
53. Tamura T, Tailor P, Yamaoka K, Kong HJ, Tsujimura H, O'Shea JJ, Singh H, Ozato K. IFN regulatory factor-4 and -8 govern dendritic cell subset development and their functional diversity. Journal of immunology. 2005; 174:2573–2581.
54. Tamura T, Yanai H, Savitsky D, Taniguchi T. The IRF family transcription factors in immunity and oncogenesis. Annual review of immunology. 2008; 26:535–584.
55. Driggers PH, Ennist DL, Gleason SL, Mak WH, Marks MS, Levi BZ, Flanagan JR, Appella E, Ozato K. An interferon gamma-regulated protein that binds the interferon-inducible enhancer element of major histocompatibility complex class I genes. Proceedings of the National Academy of Sciences of the United States of America. 1990; 87:3743–3747. [PubMed: 2111015]
56. Weisz A, Marx P, Sharf R, Appella E, Driggers PH, Ozato K, Levi BZ. Human interferon consensus sequence binding protein is a negative regulator of enhancer elements common to interferon-inducible genes. The Journal of biological chemistry. 1992; 267:25589–25596. [PubMed: 1460054]
57. Lin HK, Bergmann S, Pandolfi PP. Cytoplasmic PML function in TGF-beta signalling. Nature. 2004; 431:205–211. [PubMed: 15356634]
58. Pampin M, Simonin Y, Blondel B, Percherancier Y, Chelbi-Alix MK. Cross talk between PML and p53 during poliovirus infection: implications for antiviral defense. Journal of virology. 2006; 80:8582–8592. [PubMed: 16912307]
59. Ulbricht T, Alzrigat M, Horch A, Reuter N, von Mikecz A, Steimle V, Schmitt E, Kramer OH, Stamminger T, Hemmerich P. PML promotes MHC class II gene expression by stabilizing the class II transactivator. The Journal of cell biology. 2012; 199:49–63. [PubMed: 23007646]
60. Zhang EY, Kong KF, Altman A. The yin and yang of protein kinase C-theta (PKCtheta): a novel drug target for selective immunosuppression. Advances in pharmacology. 2013; 66:267–312. [PubMed: 23433459]
61. Giordano M, Roncagalli R, Bourdely P, Chasson L, Buferne M, Yamasaki S, Beyaert R, van Loo G, Auphan-Anezin N, Schmitt-Verhulst AM, Verdeil G. The tumor necrosis factor alpha-induced protein 3 (TNFAIP3, A20) imposes a brake on antitumor activity of CD8 T cells. Proceedings of the National Academy of Sciences of the United States of America. 2014; 111:11115–11120. [PubMed: 25024217]

62. Li Z, Li D, Tsun A, Li B. FOXP3+ regulatory T cells and their functional regulation. Cellular & molecular immunology. 2015; 12:558–565. [PubMed: 25683611]

63. van Loosdregt J, Fleskens V, Fu J, Brenkman AB, Bekker CP, Pals CE, Meerding J, Berkers CR, Barbi J, Grone A, Sijts AJ, Maurice MM, Kalkhoven E, Prakken BJ, Ovaa H, Pan F, Zaiss DM, Coffer PJ. Stabilization of the transcription factor Foxp3 by the deubiquitinase USP7 increases Treg-cell-suppressive capacity. Immunity. 2013; 39:259–271. [PubMed: 23973222]

64. Zhu Y, Chen G, Lv F, Wang X, Ji X, Xu Y, Sun J, Wu L, Zheng YT, Gao G. Zinc-finger antiviral protein inhibits HIV-1 infection by selectively targeting multiply spliced viral mRNAs for degradation. Proceedings of the National Academy of Sciences of the United States of America. 2011; 108:15834–15839. [PubMed: 21876179]

65. Bonvin M, Greeve J. Hepatitis B: modern concepts in pathogenesis--APOBEC3 cytidine deaminases as effectors in innate immunity against the hepatitis B virus. Current opinion in infectious diseases. 2008; 21:298–303. [PubMed: 18448976]

66. Chiu YL, Greene WC. The APOBEC3 cytidine deaminases: an innate defensive network opposing exogenous retroviruses and endogenous retroelements. Annual review of immunology. 2008; 26:317–353.

67. Karsan A, Yee E, Kaushansky K, Harlan JM. Cloning of human Bcl-2 homologue: inflammatory cytokines induce human A1 in cultured endothelial cells. Blood. 1996; 87:3089–3096. [PubMed: 8605321]

68. Koziczak-Holbro M, Joyce C, Gluck A, Kinzel B, Muller M, Tschopp C, Mathison JC, Davis CN, Gram H. IRAK-4 kinase activity is required for interleukin-1 (IL-1) receptor- and tolllike receptor 7-mediated signaling and gene expression. The Journal of biological chemistry. 2007; 282:13552–13560. [PubMed: 17337443]

69. Li S, Strelow A, Fontana EJ, Wesche H. IRAK-4: a novel member of the IRAK family with the properties of an IRAK-kinase. Proceedings of the National Academy of Sciences of the United States of America. 2002; 99:5567–5572. [PubMed: 11960013]

70. Suzuki N, Suzuki S, Millar DG, Unno M, Hara H, Calzascia T, Yamasaki S, Yokosuka T, Chen NJ, Elford AR, Suzuki J, Takeuchi A, Mirtsos C, Bouchard D, Ohashi PS, Yeh WC, Saito T. A critical role for the innate immune signaling molecule IRAK-4 in T cell activation. Science. 2006; 311:1927–1932. [PubMed: 16574867]

71. Morrison C, Smith GC, Stingl L, Jackson SP, Wagner EF, Wang ZQ. Genetic interaction between PARP and DNA-PK in V(D)J recombination and tumorigenesis. Nature genetics. 1997; 17:479–482. [PubMed: 9398855]

72. Chakraborty PK, Schmitz-Abe K, Kennedy EK, Mamady H, Naas T, Durie D, Campagna DR, Lau A, Sendamarai AK, Wiseman DH, May A, Jolles S, Connor P, Powell C, Heeney MM, Giardina PJ, Klaassen RJ, Kannengiesser C, Thuret I, Thompson AA, Marques L, Hughes S, Bonney DK, Bottomley SS, Wynn RF, Laxer RM, Minniti CP, Moppett J, Bordon V, Geraghty M, Joyce PB, Markianos K, Rudner AD, Holcik M, Fleming MD. Mutations in TRNT1 cause congenital sideroblastic anemia with immunodeficiency, fevers, and developmental delay (SIFD). Blood. 2014; 124:2867–2871. [PubMed: 25193871]

73. Zhao C, Beaudenon SL, Kelley ML, Waddell MB, Yuan W, Schulman BA, Huibregtse JM, Krug RM. The UbcH8 ubiquitin E2 enzyme is also the E2 enzyme for ISG15, an IFN-alpha/beta-induced ubiquitin-like protein. Proceedings of the National Academy of Sciences of the United States of America. 2004; 101:7578–7582. [PubMed: 15131269]

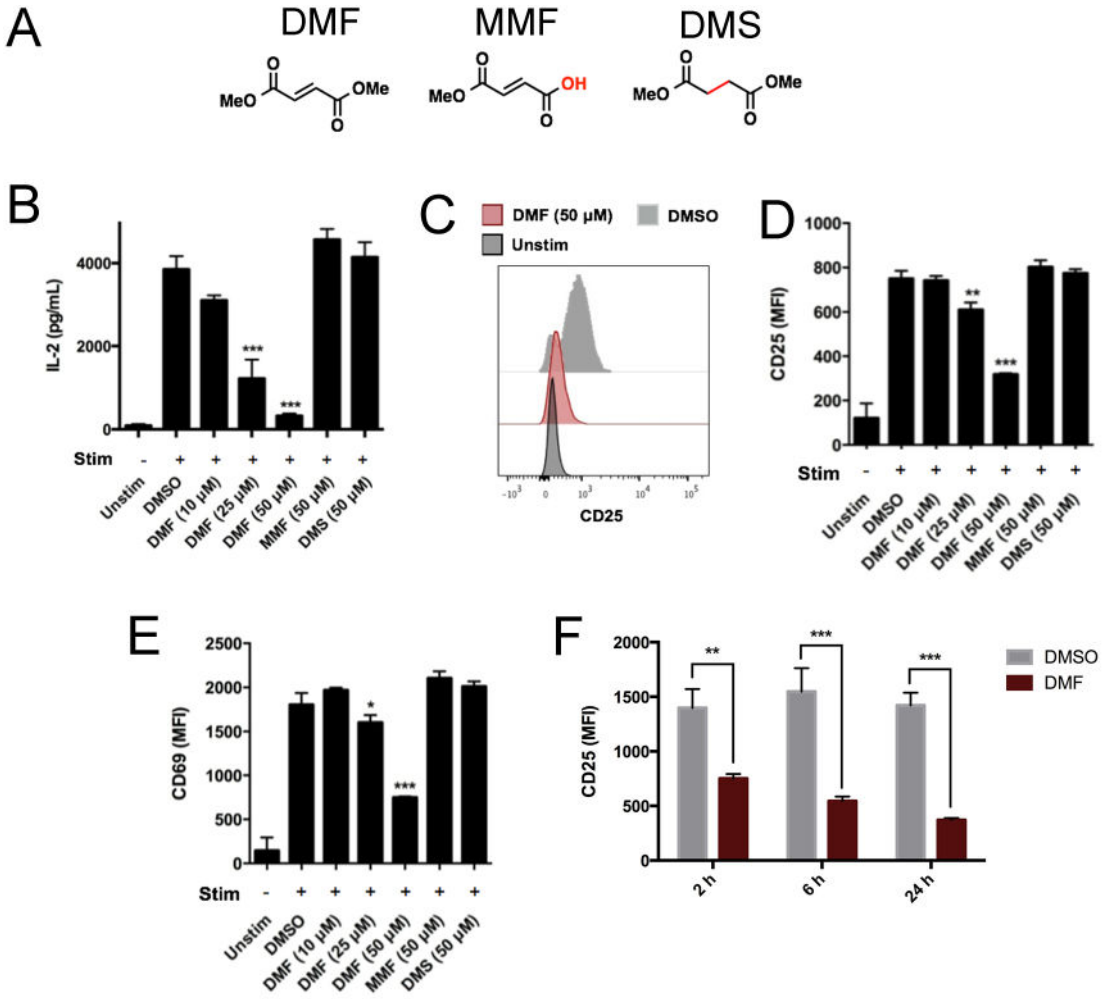

Fig. 1. DMF inhibits the activation of primary human T cells

(**A**) The chemical structures of DMF, MMF, and DMS. (**B** to **E**) Primary human T cells were left unstimulated (Unstim) or were stimulated (Stim) with anti-CD3 and anti-CD28 (anti-CD3/CD28) antibodies in the presence of DMSO or the indicated concentrations of DMF, MMF, or DMS for 8 hours. The cells were then analyzed by ELISA to determine the amount of IL-2 secreted (B) or were subjected to flow cytometric analysis of the cell surface abundance of CD25 (C and D) and CD69 (E). Flow cytometry data are presented as the mean fluorescence intensity (MFI) of the indicated markers. (**F**) Time-course analysis of the effects of DMF on CD25 abundance. Primary human T cells were stimulated with anti-CD3/CD28 antibodies in the presence of DMSO or DMF for the indicated times before the DMF-containing medium was replaced with DMF-free medium. The cells were harvested 24 hours after T cell stimulation was begun. The cell-surface abundance of CD25 was measured on gated $CD4^+$ T cells. Data in (B) and (D) to (F) are means ± SEM of four to six technical replicates from each of two experiments. $*P < 0.05$, $**P < 0.01$, $***P < 0.001$ by two-tailed, unpaired *t* test in comparison to the DMSO-treated cells.

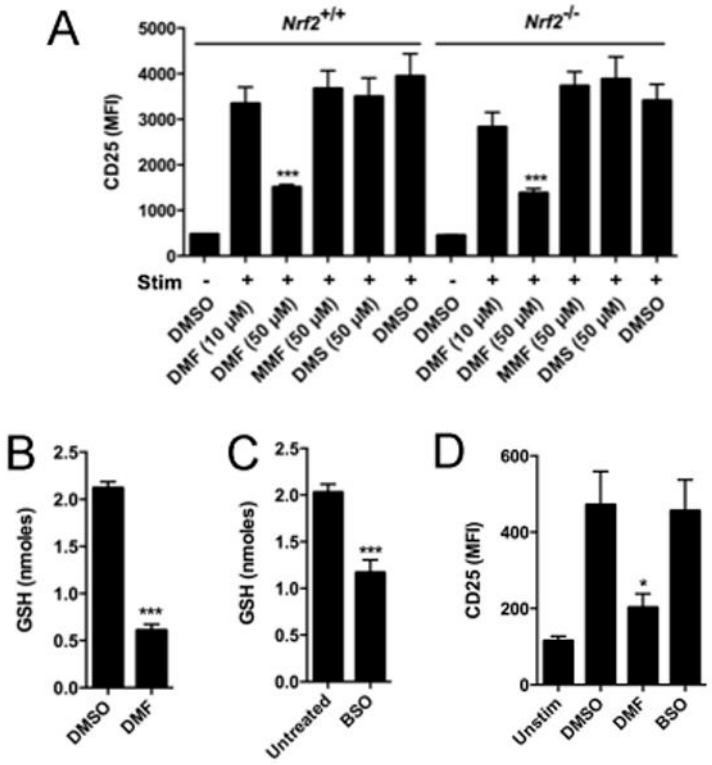

Fig. 2. The inhibitory effects of DMF are equivalent in *Nrf2*$^{+/+}$ and *Nrf2*$^{-/-}$ T cells and are not caused by reductions in cellular GSH abundance

(**A**) Total splenic T cells from *Nrf2*$^{+/+}$ and *Nrf2*$^{-/-}$ mice were left unstimulated or were stimulated with anti-CD3/CD28 antibodies in the presence of the indicated compounds for 24 hours. The cells were then analyzed by flow cytometry to determine the cell surface abundance of CD25. (**B** and **C**) DMF and BSO markedly reduce the amount of GSH in human T cells. Primary human T cells were stimulated with anti-CD3/CD28 antibodies in the presence of 50 μM DMF for 2 hours (B) or 2.5 mM BSO for 4 hours (C), after which intracellular GSH concentrations were measured. (**D**) BSO does not alter T cell activation. Primary human T cells were left unstimulated or were stimulated with anti-CD3/CD28 antibodies in the presence of DMSO, 50 μM DMF, or 2.5 mM BSO for 8 hours. The cells were then analyzed by flow cytometry to measure the cell-surface abundance of CD25. Data are means ± SEM of three or four technical replicates from each of two experiments. *$P <$ 0.05, **$P < 0.01$, ***$P < 0.001$ by two-tailed, unpaired *t* test, in comparison to the DMSO-treated cells.

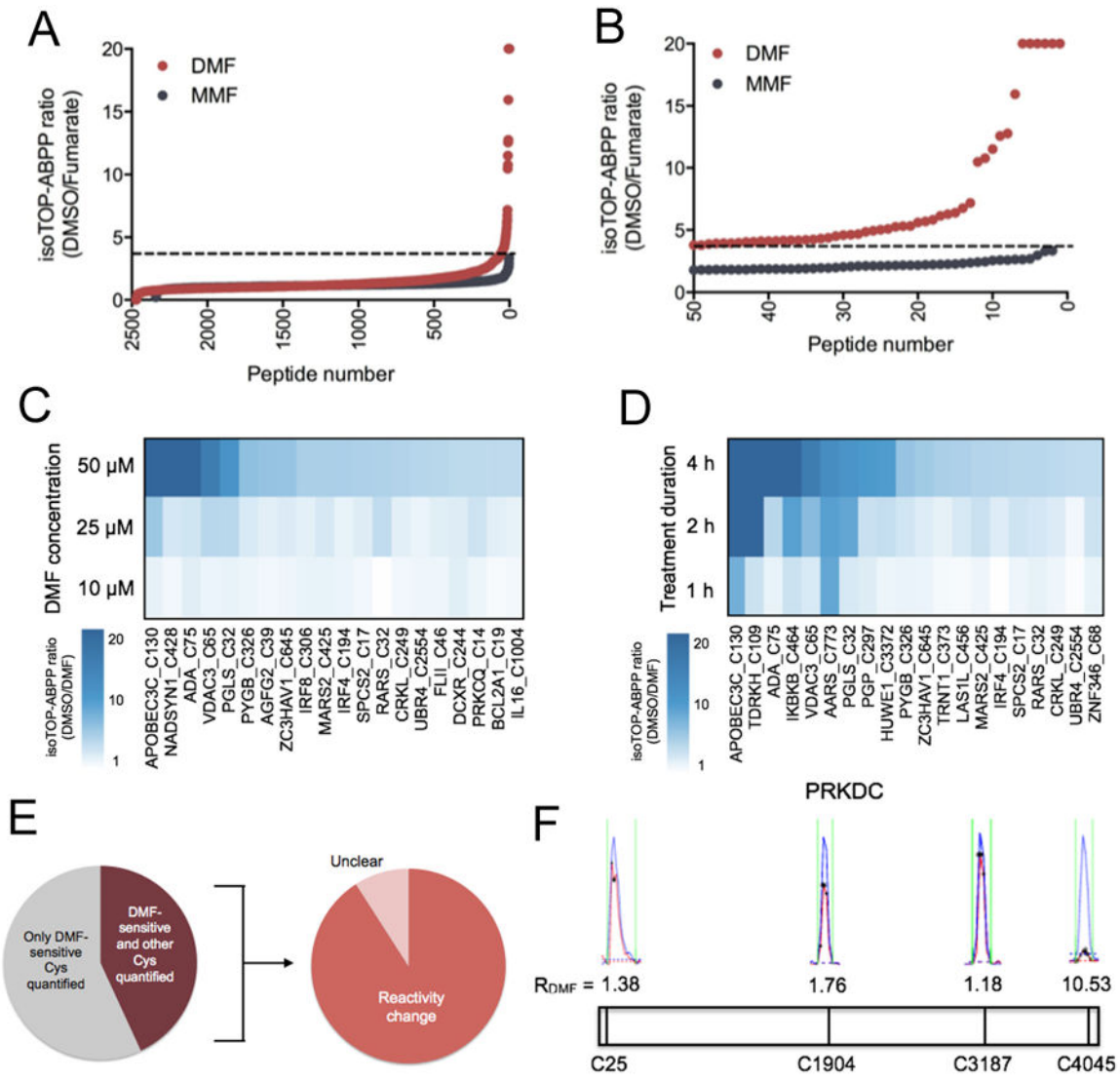

Fig. 3. Analysis of DMF-treated primary human T cells by isoTOP-ABPP

(**A**) isoTOP-ABPP ratios, or R values, for > 2400 cysteine residues in primary human T cells that were activated with anti-CD3/CD28 antibodies and treated for four hours with DMSO, 50 μM DMF, or 50 μM MMF. (**B**) Expanded profile for DMF-sensitive cysteine residues, where sensitivity is defined as a > four-fold reduction in IA-alkyne reactivity in DMF-treated vs. DMSO-treated T cells (DMSO/DMF R value > 4). For (A) and (B), data represent aggregate quantified cysteine residues from five biological replicates. For the cysteine residues quantified in more than one replicate, average ratios are reported. The dashed line designates R values > 4. (**C** and **D**) Concentration-dependent (C) and time-dependent (D) R values for DMF-sensitive cysteine residues in primary human T cells. Each column corresponds to an individual DMF-sensitive cysteine residue, and each tile represents the average R value for that cysteine residue in isoTOP-ABPP experiments performed at the indicated concentration of DMF (concentration-dependence treatments were performed for 4 hours) or duration of treatment (time course treatments were performed with 50 μM DMF). (**E**) Left: Fraction of proteins for which both a DMF-sensitive

cysteine residue and at least one additional cysteine residue was quantified. Right: Fraction of these proteins in which the additional cysteine residue was unchanged (DMSO/DMF R value < 2.0). Unclear calls mark proteins with DMF-sensitive cysteine residues and for which the R value for the second cysteine showed marginal evidence of a potential change (R values between 2.0 and 3.9). (**F**) Representative MS1 profiles for quantified cysteine residues in PRKDC, one of which (Cys^{4045}) showed sensitivity to DMF. Blue indicates the DMSO-treated sample (heavy isotopic tag); red indicates the DMF-treated sample (light isotopic tag). Asterisks represent MS2 events that were recorded by the MS instrument.

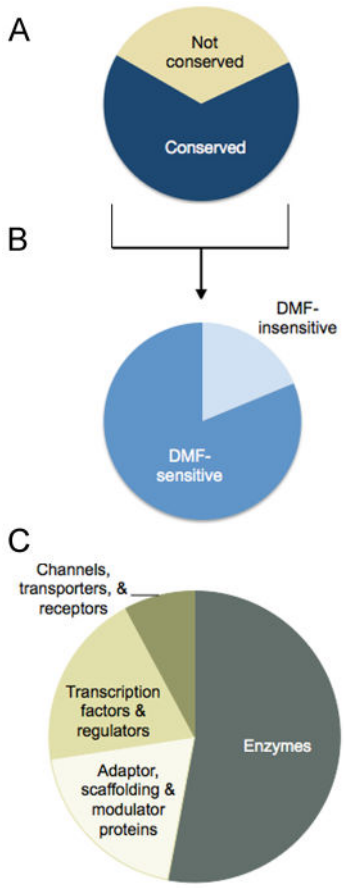

Fig. 4. Conservation and functional analysis of DMF-sensitive cysteines

(**A**) Fraction of the DMF-sensitive cysteine residues in the human T cell proteome that are conserved in mice. (**B**) Fraction of conserved DMF-sensitive cysteine residues in human T cells that were quantified and also sensitive to DMF in mouse T cells. (**C**) Distribution of proteins in primary human T cells harboring DMF-sensitive cysteine residues by functional class.

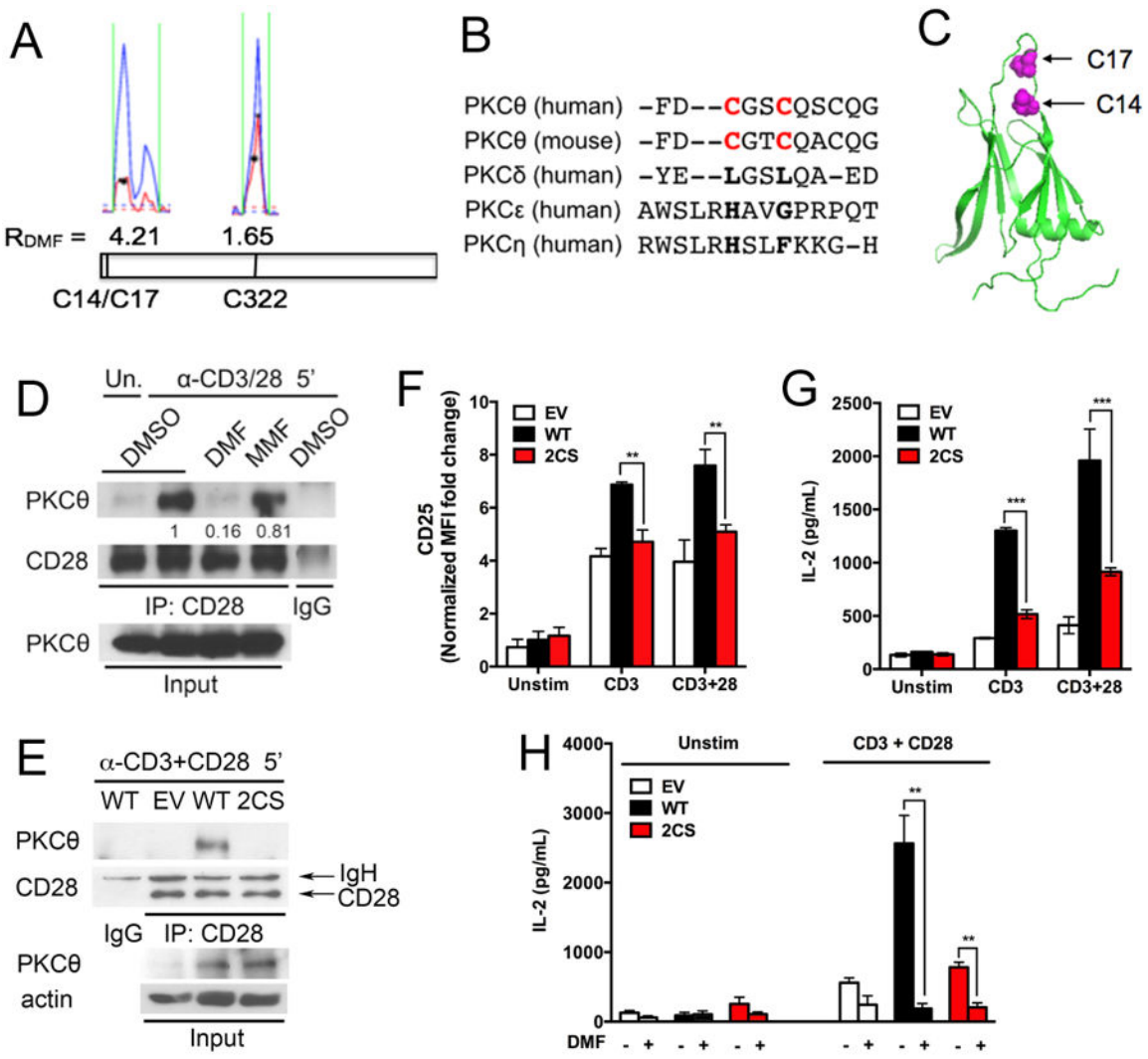

Fig. 5. The DMF-sensitive residues Cys^{14} and Cys^{17} in PKC0 are required for its interactions with CD28 and for T cell activation

(**A**) Representative MS1 profiles for DMF-sensitive (Cys^{14} and Cys^{17}) and -insensitive (Cys^{322}) cysteine residues in PKCθ. Blue indicates the DMSO-treated sample (heavy isotopic tag); red indicates the DMF-treated sample (light isotopic tag). Asterisks represent MS2 events recorded by the MS instrument. (**B**) Sequence conservation analysis of human and mouse PKCθ, human PKCδ, human PKCε, and human PKCη. Cys^{14} and Cys^{17} are in red. (**C**) Location of the DMF-sensitive residues Cys^{14} and Cys^{17} in the C2 domain of human PKCθ (PDB accession number 2ENJ). (**D**) DMF, but not MMF, blocks the association of PKCθ with CD28. Peripheral CD4^{+} T cells from C57BL/6 mice were pre-incubated with DMSO, 50 μM DMF, or 50 μM MMF and then were left unstimulated or were stimulated with anti-CD3/CD28 antibodies for 5 min. The cells were washed, lysed, subjected to immunoprecipitation (IP) with anti-CD28 or control IgG antibodies, and then analyzed by Western blotting with antibodies specific for CD28 and PKCθ. Whole-cell lysates (Input) were also analyzed. Western blots are representative of four experiments. Quantification of band intensities from multiple experiments is shown in fig. S7A. (**E**)

PKCθ$^{-/-}$ T cells were reconstituted with control retrovirus (EV), retrovirus encoding wild-type (WT) PKCθ, or retrovirus encoding the 2CS PKCθ mutant. The cells were then stimulated with anti-CD3/CD28 antibodies for 5 min before being lysed and subjected to immunoprecipitation with anti-CD28 or IgG antibodies. Immunoprecipitated samples and whole-cell lysates (Input) were then analyzed by Western blotting with antibodies against the indicated targets. Western blots are representative of three experiments. Quantification of band intensities from multiple experiments is shown in fig. S7B. (**F** and **G**) PKCθ$^{-/-}$ T cells reconstituted with WT PKCθ or the 2CS mutant PKCθ were left unstimulated or were stimulated with anti-CD3 antibody alone or in the presence of anti-CD28 antibody. The cells were then analyzed by flow cytometry to determine the cell-surface abundance of CD25 (F) or by ELISA to measure the amount of secreted IL-2 (G). (**H**) PKCθ$^{-/-}$ T cells reconstituted with empty vector, WT PKCθ, or the 2CS mutant PKCθ were left unstimulated or were stimulated with anti-CD3/CD28 antibodies overnight in the presence or absence of 50 μM DMF. Cell culture medium was then analyzed by ELISA to measure the amount of secreted IL-2. For (E) to (H), PKCθ$^{-/-}$ T cells were pre-activated with plate-coated anti-CD3/CD28 antibodies for 24 hours before undergoing retroviral transduction. The cells were rested in culture medium without stimulation for 48 hours and then were incubated with or without plate-coated anti-CD3/CD28 antibodies (1 μg/ml) overnight (F) or for 48 hours (G and H), or with soluble anti-CD3/CD28 antibodies (10 μg/ml) for 5 min before being subjected to immunoprecipitation (E). Data in (F) to (H) are means ± SEM of three biological replicates. $*P < 0.05$, $**P < 0.01$, $***P < 0.001$ by two-tailed, unpaired *t* test.